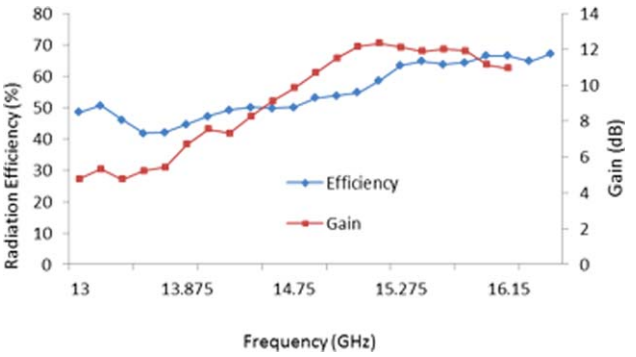

Figure 8 Maximum Gain over frequency for the grid antenna. [Color figure can be viewed at wileyonlinelibrary.com]

result indicates that the antenna achieved a bandwidth of 2.1 GHz covering the frequencies of 13.8 GHz to 15.9 GHz.

Figure 6 and Figure 7, respectively, depict the radiation pattern for the measured and simulated antenna in H-Plane and E-Plane. In both the E-Plane and H-Plane, the antenna has its maximum radiation along the boresight direction. It can be seen that there is a good agreement between the measured and simulated results for the radiation pattern of the antenna.

A plot of gain and efficiency of the antenna both as functions of frequency is presented in Figure 8. Based on the plot, a maximum directive gain of 12.7 dB (14.4 dBi) and maximum efficiency of 66% at 15.9 GHz has been achieved by the antenna.

5. CONCLUSION

A 15 GHz, compact and high gain grid array antenna for 5G mobile communication is reported. It is implemented on an FR4 substrate and has achieved an impedance bandwidth of 2.1 GHz from 13.8 GHz to 15.9 GHz. The antenna has also achieved a gain of 14.4 dBi at 15.9 GHz. This gain is higher than that of the previously reported grid array antennas for 5G mobile communications systems. It is therefore a good candidate for 5G mobile communications covering the 5G proposed band of 14.4–15.35 GHz.

REFERENCES

1. W.S. Chen, B.Y. Lee, and Y.T. Liu, A printed coupled-fed loop antenna with two chip inductors for the 4G mobile applications, Microw Opt Technol Lett 54 (2012), 2157–2163.
2. W.S. Chen, B.Y. Lee, and Y.T. Liu, A coupled-fed loop antenna for fourth generation mobile system applications, Microw Opt Technol Lett 54 (2012), 1900–1907.
3. Y.K. Bekali and M. Essaaidi, Compact reconfigurable dual frequency microstrip patch antenna for 3G and 4G mobile communication technologies, Microw Opt Technol Lett 55 (2013), 1622–1626.
4. M. A. Albreem, 5G wireless communication systems: Vision and challenges, In: International Conference on Computer, Communications, and Control Technology, IEEE, (2015), pp. 493–497.
5. S. Hakimi, S.K.A. Rahim, Millimeter-wave microstrip Bent Line grid array antenna for 5G mobile communication networks, In: Asia-Pacific Microwave Conference Proceedings, IEEE, 2014, pp. 622–624.
6. L. Zhang, Y.P. Zhang, and Y.L. Lu, A 24-GHz microstrip grid array antenna, In: International Symposium on Antennas and Propagation Proceedings, IEEE, Chicago, IL, 2012.
7. X. Chen, G. Wang, and K. Huang, A novel wideband and compact microstrip grid array antenna, IEEE Trans Antennas Propag 58 (2010), 596–599.
8. Z. Chen, and Y.P. Zhang, FR4 PCB grid array antenna for millimeter-wave 5G mobile communications, In: Microwave Workshop Series on RF and Wireless Technologies for Biomedical and Healthcare Applications, IEEE pp. 1–3.
9. M. Sun, Y.P. Zhang, D. Liu, K.M. Chua, and L.L. Wai, A ball grid array package with a microstrip grid array antenna for a single-chip 60-GHz receiver, IEEE Trans Antennas Propag 59 (2011), 2134–2140.
10. O. Khan, J. Pontes, X. Li, and C. Waldschmidt, A wideband variable width microstrip grid array antenna, In: European Microwave Conference, IEEE, 2014, pp. 1644–1647.
11. H. Nakano, I. Oshima, H. Mimaki, K. Hirose, and, J. Yamauchi, Centerfed grid array antennas, In: Antennas and Propag Society International Symposium, Newport Beach, CA, IEEE, 1995.
12. L. Zhang, Y.P Zhang, and Y. Lu, 30-dBi gain microstrip grid array antenna at 24 GHz on a single-layer substrate, In: Antennas and Propag Society International Symposium, IEEE, 2013.

BACKSCATTERING TECHNIQUE FOR REAL-TIME MONITORING OF THE RECEIVED POWER IN WIRELESS POWER TRANSMISSION SYSTEMS

Telnaz Zarifi,[1] Kambiz Moez,[2] and Pedram Mousavi[3]
[1] Electrical and Computer Engineering, University of Alberta, Edmonton, Alberta, Canada T6G 1H9; Corresponding author: telnaz@ualberta.ca
[2] Electrical and Computer Engineering, University of Alberta
[3] Department of Mechanical Engineering

Received 23 May 2016

ABSTRACT: *A wireless power transmission system with a dynamic, real-time feedback for impedance matching is presented. The AC signal at the receiver node is rectified, the resulting DC signal is passed to a voltage controlled oscillator which drives a high-frequency analog switch. When in the ON state, the switch shorts the terminals of the receiver coil, dramatically changing the impedance seen by the transmitter coil. This change is detected on the transmitter side as the backscattered signal. Variation on the frequency of the backscattered signal can then be used to affect changes in the power source amplitude or the transmission side matching network to optimize the transmission power efficiency. The proposed feedback system is implemented with planar spiral coils on PCBs, and the effect of distance variation between the coils and as a consequence, DC voltage variation on the rectifier output is measured using voltage signal spectrum in the transmitter node at 1 MHz.* © 2016 Wiley Periodicals, Inc. Microwave Opt Technol Lett 58:2980–2983, 2016; View this article online at wileyonlinelibrary.com. DOI 10.1002/mop.30189

Key words: *wireless power transmission; backscattering; voltage control oscillator; doubler rectifier*

1. INTRODUCTION

Wireless power transmission (WPT) is an effective method of delivering electric power to inaccessible loads in various environments. This method has been used to deliver electric power to sensors, readout circuits, and power storage devices in various biomedical, industrial, and environmental applications [1–3]. In WPT systems, an electromagnetic field transmits electric power from source to receiver nodes through an electrically nonconductive medium. This technique delivers electric power and signals from a transmitter to several receiver nodes via three main principles: electric or magnetic coupling for near field applications, and electromagnetic coupling for far field applications [4].

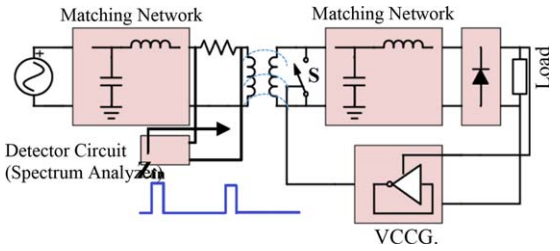

Figure 1 System level architecture of the designed WPT system[TQ2]. [Color figure can be viewed at wileyonlinelibrary.com]

One of the challenges in WPT systems is to maximize the power transmission efficiency (PTE) from a transmitter to a receiver node, and several techniques have been investigated to address this issue. Resonance inductive coupling (RIC) is a very popular and widely used method. This method utilizes resonant coils both in transmitter and receiver and improves the directivity and PTE considerably [5]. However, misalignment and distance variation between the transmitter and receiver coils can significantly degrade the PTE by changing the power level as a consequence of coupling inductance variation or frequency splitting phenomena [6].

One of the effective techniques which is proposed for real-time efficiency enhancement is an automated impedance matching (IM) system. In this method, adjustable parameters such as the capacitor or inductor values in the IM circuit are manipulated to obtain the maximum transmitted power efficiency. Beh *et al*. have demonstrated a PTE of 85% by employing an automated matching circuit using a simple best step steepest descent method search algorithm. The proposed algorithm with the WPT system operates at 13.56 MHz, employing a directional coupler to measure the reflected wave ratio at the transmitting end of the system. It then employs high-frequency relays to select the matching parameters required to minimize the reflected wave [7]. Enhancement of the PTE using a resonator-controller combination at the receiver side has been reported by Ahn and Hong. The proposed technique demonstrated a 9% improvement for a 20-W loading at a coil-distance of 15 cm for a 20 cm $\times$ 16 cm receiver [8].

In this paper, we demonstrate a real-time feedback system for monitoring the received power level in a WPT system with RIC using the backscattered signal in the transmitter node. Voltage Controlled Clock Generator (VCCG) is employed to control the ON/OFF state of the shunt switch, which is placed in parallel with the receiver coil to create a backscatter signal. The clock frequency of the VCCG depends on the DC voltage level of the rectifier output signal. Because of the electromagnetic coupling between the transmitter and receiver coils, a dramatic variation of the load in the receiver node produces corresponding impedance changes across the transmitter coil and generates a backscattered feedback signal. As the switching frequency of backscattered signal in the transmitted node represents the DC voltage level in the receiver output, it can be effectively used to control the amplitude of the transmitted power by adjusting the power level of the source and adaptively adjusting the matching network's variable components in the transmitter node to effectively control the power delivery to a load in WPT system.

2. SYSTEM DESIGN AND SIMULATIONS

A WPT system compose of transmitter and receiver coils, which are associated with impedance matching networks. In the receiver node, an AC to DC converter, such as doubler rectifier, converts the sinusoidal received signal to DC voltage. To enable real-time monitoring of the received power levels, a VCCG is added to generate a variable frequency clock signal depending on the rectified DC voltage along with a shunt switch to create backscatter signal. At the transmitter, a detector circuit is added to detect the corresponding changes in the input impedance of transmitting coil to retrieve the backscattered signal (Fig. 1).

An analog switch controlled by the clock signal from the VCCG's output is placed is in parallel with the receiver coil. The system operates normally when the analog switch is in the OFF-state rectifying the received signal to a DC voltage. When the switch is in its ON-state, the terminals of the receiver resonant coil are shorted, which dramatically changes the impedance seen by the transmitter coil. The impedance variation in the transmitted side can be monitored through variations in the reflected power. In the designed system, the impedance variation frequency in the transmitter side is related to the DC voltage level at the rectifier output in the receiver node. This relationship is established by using the voltage controlled switch at the front-end of the receiver node. Electromagnetic (EM) simulation in HFSS for two coupled coils demonstrates the effects of the short/open states of the switch on the magnetic field distribution and amplitude in between the transmitter and receiver coils (Fig. 2).

To verify the switching effect of the shunt switch of the receiver coil on the input impedance of the transmitter coil (Z_{in}) in variant distances, 3D electromagnetic simulations are performed. For three different distances between the transmitter and receiver coils, the S_{11} and Z_{in} parameters are studied in the short and open switch states (Fig. 3). The transmitter node can track the DC voltage variation at the receiver node by detecting the backscattered signal following its impedance variation on the transmitter side. To minimize the power delivery interruption in the ON-state of the switch, the duty cycle of the clock signal is set to 2% at 1 MHz. An XOR gate oscillator is implemented with RC elements along with spike generation circuit to fulfill the required delay and to convert the output DC voltage to clock signal with adjustable duty cycle (Fig. 4).

3. SYSTEM IMPLEMENTATION, RESULTS, AND DISCUSSION

The proposed circuit and coil structures are implemented on a RT 5880 substrate from Rogers Corporation. The substrate has relative permittivity of 2.2 with loss factor of 0.0003 and thickness of

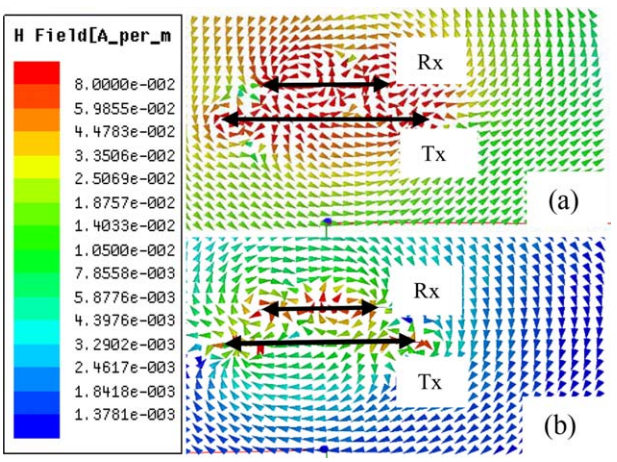

Figure 2 The magnetic field between the transmitter and receiver coils at a distance of 20 cm, (a) presents the field amplitude and distribution with the switch in the open-state, (b) demonstrates the magnetic field when the switch is in the short-state. [Color figure can be viewed at wileyonlinelibrary.com]

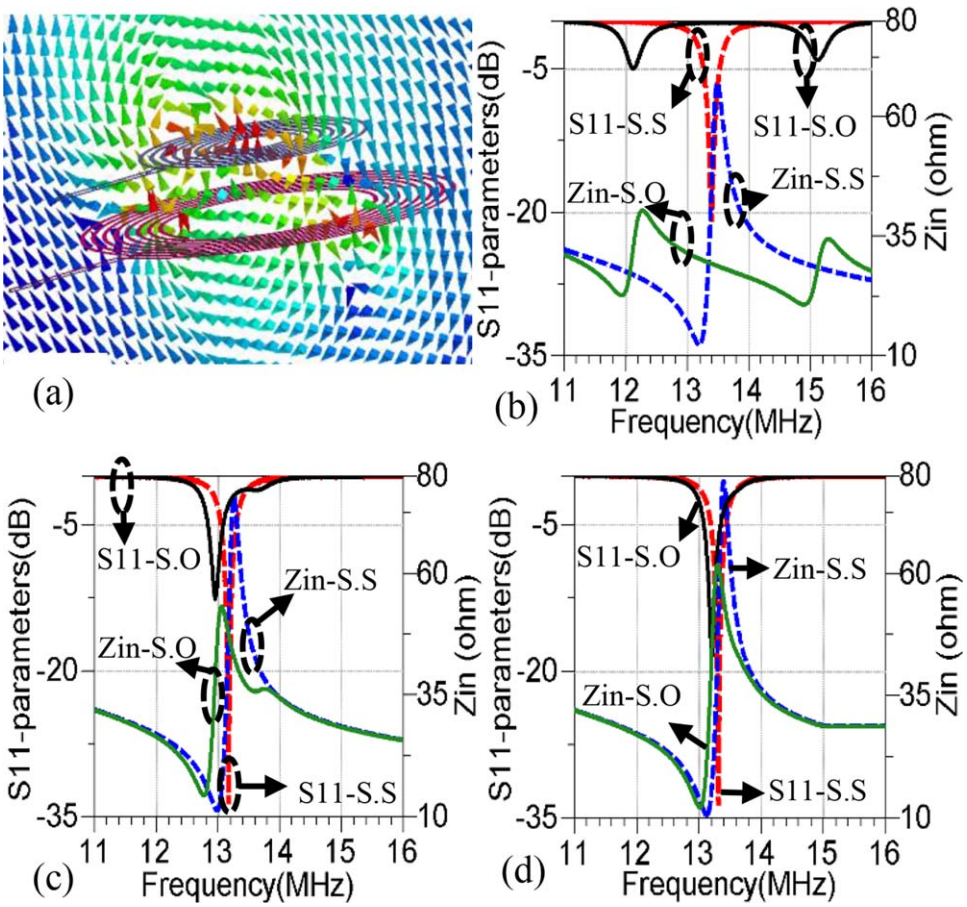

Figure 3 (a) Two coupled coils in HFSS, S_{11} and T_x coil input impedance (Z_{in}) in switch short (S.S.) and switch open (S.O.) for, (b) 20 mm, (c) 70 mm, and (d) 100 mm. [Color figure can be viewed at wileyonlinelibrary.com]

0.79 mm. The planar spiral coils has a trace width of 1 mm, a trace gap of 1 mm, and inner and outer diameters of 42 and 94 mm, respectively. A three-stage voltage double rectifier is implemented to perform the AC to DC signal conversion. HSMS-2820 diodes from Avago-technologies with a low forward bias voltage of 0.3 V are used in the rectifier structure. The VCCG circuit is realized using XOR-logic gate and Schmitt trigger NOT-logic, 74LS86, 74LS14 with R and C delay elements of 10 Ω and 47 pF, respectively. The implemented coils and circuits with the experimental test-setup are shown in Figure 5.

The S_{11}-parameter in the transmitter node is investigated for open and short states of the switch (S) at three different distances of 5, 7, and 10 cm. As shown in Figure 6, the backscattering has a significant affect on the S_{11} of the transmitter in the presented range of distance between T_x and R_x coils.

To confirm the functionality of the proposed system, the frequency spectrum of the current flowing through the transmitter coil is measured by converting to voltage passing through a resistor [Fig. 7(a)]. The oscillation frequency is designed to depend on the output DC voltage of the rectifier and, consequently, related to the distance between the T_x and R_x coils [Fig. 7(b)]. The oscillator's output frequency has backscatter effect on the T_x-coil signal which is used as a real-time indicator for T_x and R_x coils distances [Fig. 7(c)]. The switching frequency of the front switch (MAX4644), which is the source of the back-scattered signal, is determined by the output frequency of the VCCG. Changes in the VCCG's frequency consequently has

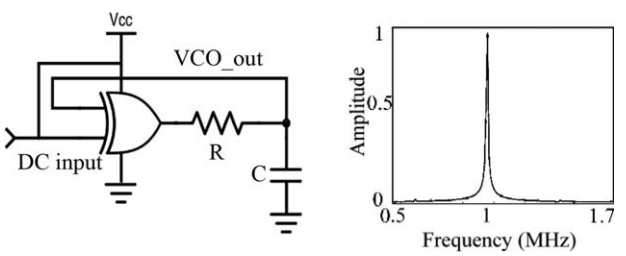

Figure 4 VCO realization circuit model and PSpice simulation results

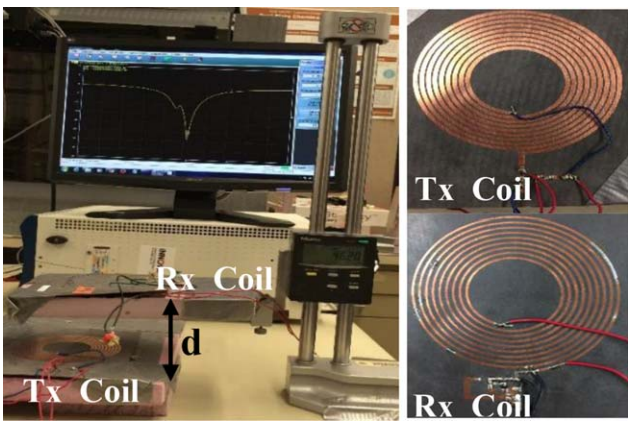

Figure 5 Experimental setup for S_{11} measurement in different distances with the implemented T_x and R_x coils. [Color figure can be viewed at wileyonlinelibrary.com]

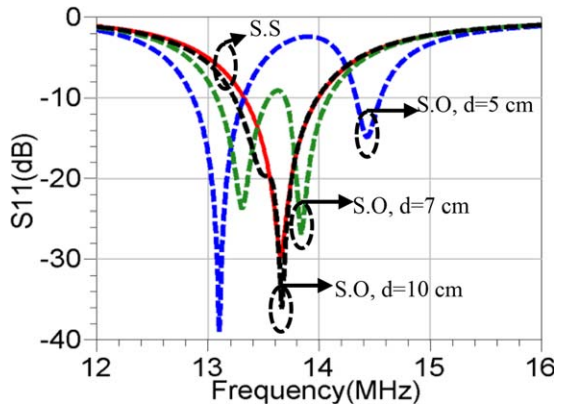

Figure 6 Measured S_{11}-parameters for short (S.S) and open (S.O) switch states from T_x coil in three distances of 5, 7, and 10 cm for the switch in short state all S_{11}-parameters are almost identical and independent from the R_x coil distance. [Color figure can be viewed at wileyonlinelibrary.com]

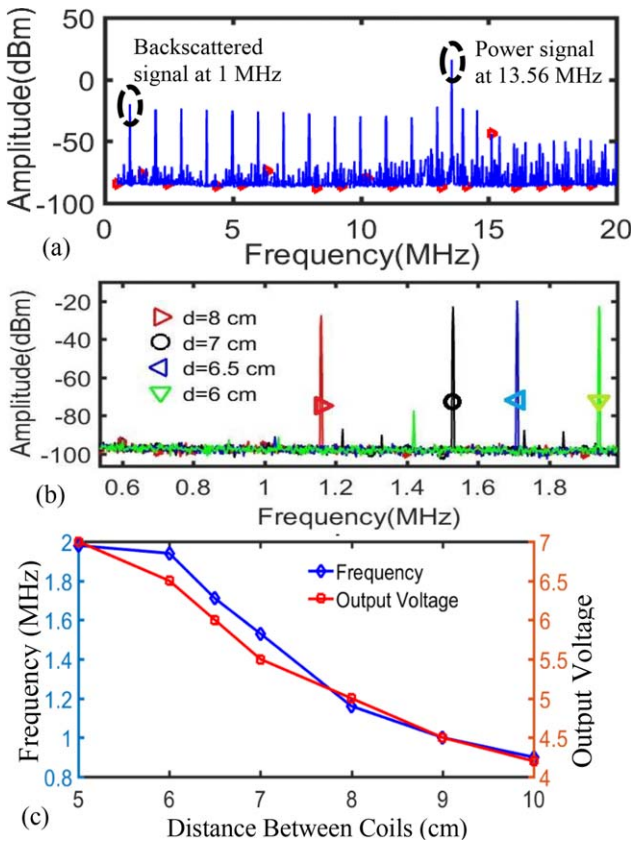

Figure 7 Spectrum measured results for varying the distance between the T_x and R_x coils, (a) full signal spectrum, power transfers at 13.56 MHz and backscattered signal at 1 MHz, (b) effect of distance variation on the frequency of the scattered signal, (c) frequency and rectifier DC output versus T_x and R_x coils distance. [Color figure can be viewed at wileyonlinelibrary.com]

a fluctuating effect on the input impedance of the transmitter coil at the transmitter node.

4. CONCLUSION

In this paper a wireless power transmission system with a dynamic, real-time feedback system is presented. The output DC-signal of the three-stage voltage multiplier is utilized as the feedback signal which controls the clock frequency of the VCCG. The output signal of the VCCG governs the switching frequency of the front switch to wirelessly translate the DC voltage level at the rectifier output in the receiver node to the transmitter node. Using the backscattered signal in the transmitter, dynamic variations of the received power in the receiver node can be continuously monitored. In addition, the transmitted power level and efficiency can be controlled by changing the amplitude of the power source or by altering the impedance matching network in the transmitter node. The reported system operates at 13.56 MHz, the backscattering signal has variation frequency range of 0.98 MHz at 1 MHz. Dynamic and real-time monitoring of the DC power is achieved in cost of 3% drop of the received power in comparison with a WPT with no-feedback system.

REFERENCES

1. J. Albesa, M. Gasulla, T. Jäger, and L.M. Reindl, Wireless power transmission for autonomous sensors in removable vehicle seats, IEEE Veh Technol Conf (2011), 1–5.
2. L. Angrisani, F. Bonavolonta, G. D'Alessandro, and M. D'Arco, Inductive power transmission for wireless sensor networks supply, IEEE Workshop Environ Energy, Struct Monit Syst Proc (2014), 1–5.
3. X. Cao, X. Zhou, L. Liu, and Y. Cheng, Energy-efficient spectrum sensing for cognitive radio enabled remote state estimation over wireless channels, IEEE Trans Wireless Commun 14 (2015), 2058–2071.
4. OSHA, Cincinnati Technical Center (May 20, 1990), Electromagn. Radiat. How It Affect. Your Instruments. Near F. vs. Far field, US Dept Labor, Washington, DC.
5. T. Nagashima, X. Wei, and H. Sekiya, Analytical design procedure for resonant inductively coupled wireless power transfer system with class-DE inverter and class-E rectifier, IEEE Asia Pac Conf Circuits Syst (2014), 288–291.
6. M. Kung and K. Lin, Enhanced analysis and design method of dual-band coil module for near-field wireless power transfer systems, IEEE Trans Microw Theory Tech 63 (2015), 821–832.
7. T.C. Beh, M. Kato, T. Imura, S. Oh, and Y. Hori, Automated impedance matching system for robust wireless power transfer via magnetic resonance coupling, IEEE Trans Ind Electron 60 (2013), 3689–3698.
8. D. Ahn and S. Hong, Wireless power transfer resonance coupling amplification by load-modulation switching controller, IEEE Trans Ind Electron 62 (2015), 898–909.

COMPACT 1 × 4 PATCH ANTENNA ARRAY BY MEANS OF EBG STRUCTURES WITH ENHANCED BANDWIDTH

Shahrokh Jam and Hossein Malekpoor
Department of Electrical and Electronic Engineering, Shiraz University of Technology, Shiraz 71555-313, Iran; Corresponding author: jam@sutech.ac.ir

Received 1 May 2016

ABSTRACT: *In this paper, a novel design of compact 1 × 4 patch antenna array using electromagnetic band gap (EBG) for wideband operation is introduced. Three unequal arms fed by CPW-to-slotline through a coupling system of 100 Ω T-shaped slotline transitions are utilized for broadening the impedance bandwidth with multiple resonances. By adding two conventional mushroom-type EBG (CMT-EBG) structures on both sides of 100 Ω slotline transitions, dual wideband patch array is obtained. The proposed 1 × 4 patch array with CMT-EBG includes two bands with the measured ranges ($S_{11} \leq -10$ dB) of*